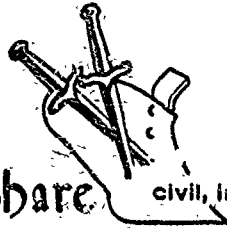PNE-1118

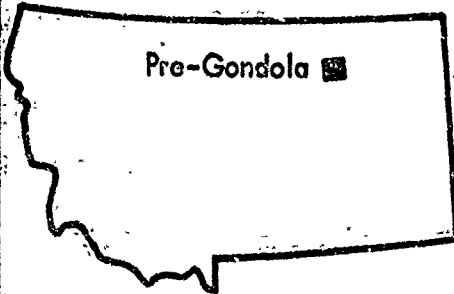**Plowshare** civil, industrial and scientific uses for nuclear explosives

UNITED STATES ARMY CORPS OF ENGINEERS

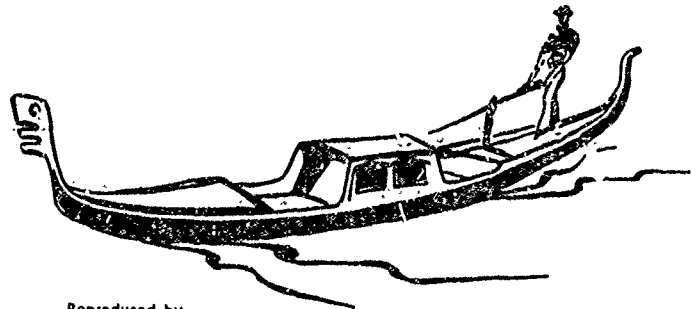FORT PECK RESERVOIR
MONTANA

Pre-Gondola ▧

PROJECT
PRE-GONDOLA III

PHASE II

MICROBAROGRAPH MEASUREMENTS

Jack W. Reed

Sandia Laboratories, Albuquerque, New Mexico

DDC
MAY 10 1972
C

U. S. Army Engineer Nuclear Cratering Group
Livermore, California

June 1971

PROJECT PRE-GONDOLA III PHASE II MICROBAROGRAPH MEASUREMENTS

Jack W. Reed

Sandia Laboratories
Albuquerque, New Mexico

June 1971

Abstract

Four microbarograph stations recorded waves at a range of approximately 130 mi from a row charge of high explosives buried near optimum cratering depth. Comparison with propagations from three airburst calibration detonations showed that a source model derived from close-in data was appropriate for distant effects predictions. This model predicted that wave amplitudes from explosives at this scaled depth would be 20% of amplitudes expected for a free-air burst. All amplitudes perpendicular to a row charge are proportional to the 0.7 power of the number of charges in the row.

PROJECT PRE-GONDOLA III PHASE II
MICROBAROGRAPH MEASUREMENTS

Project Pre-Gondola III Phase II

Pre-Gondola experiments were carried out near the west shore of Fort Peck Reservoir, Montana. The crater from this particular event, a single row detonation of buried nitromethane explosives, was designed to connect to a preexisting crater, Pre-Gondola II (excavated June 28, 1967).[1] Pre-Gondola III Phase II consisted of seven 30-ton spheres of nitromethane explosive buried in weak, wet Bearpaw clay shale, at depths and charge spacings expected to optimize cratering. Detonation was on schedule at 1000 MST, October 30, 1968. The Pre-Gondola project was conducted by the U. S. Army Engineer Nuclear Cratering Group, located at Livermore, California.

Microbarography

The purpose of the microbarograph measurements in this project was to gain further information about the long-range propagation of airblast waves from explosive cratering events, information that could be applied to the safety analyses of AEC-Plowshare nuclear explosive excavations. In particular, Phase II of Pre-Gondola III provided the first opportunity to observe propagations at long range, perpendicular to a row-charge detonation, and in a direction of expected high-altitude ozonosphere sound ducting.[2] In previous large row-charge experiments rows were aligned nearly east-west.[3,4] Only relatively weak waves, emitted off the ends, were propagated great distances by prevailing seasonal east or west winds at approximately 150,000-ft altitudes. Much stronger waves are emitted perpendicular to a row charge,[5,6] and, with north-south orientation of bursts postulated by Inter-oceanic Canal Studies, east or west is the direction of blast-ducting winds and is over land where nuisance level damage and hazards could result. An immediate goal was to establish whether nearly acoustic wave addition, found from close-in airblast measurements on small charge experiments, was also operative at downwind ranges of approximately a hundred miles where concentrations of ozonosphere-ducted sound usually appear.

Operations Plan

Four microbarograph stations were operated at a range of approximately 130 mi in about northeast through southeast directions. It was expected that winter westerly winds would have become established at high altitudes by late October and duct the airblast wave into these stations.[7] The locations of the stations are shown in Fig. 1. Shot-to-station bearings and separations are listed in Table 1. Locations

Table 1. Microbarograph locations.

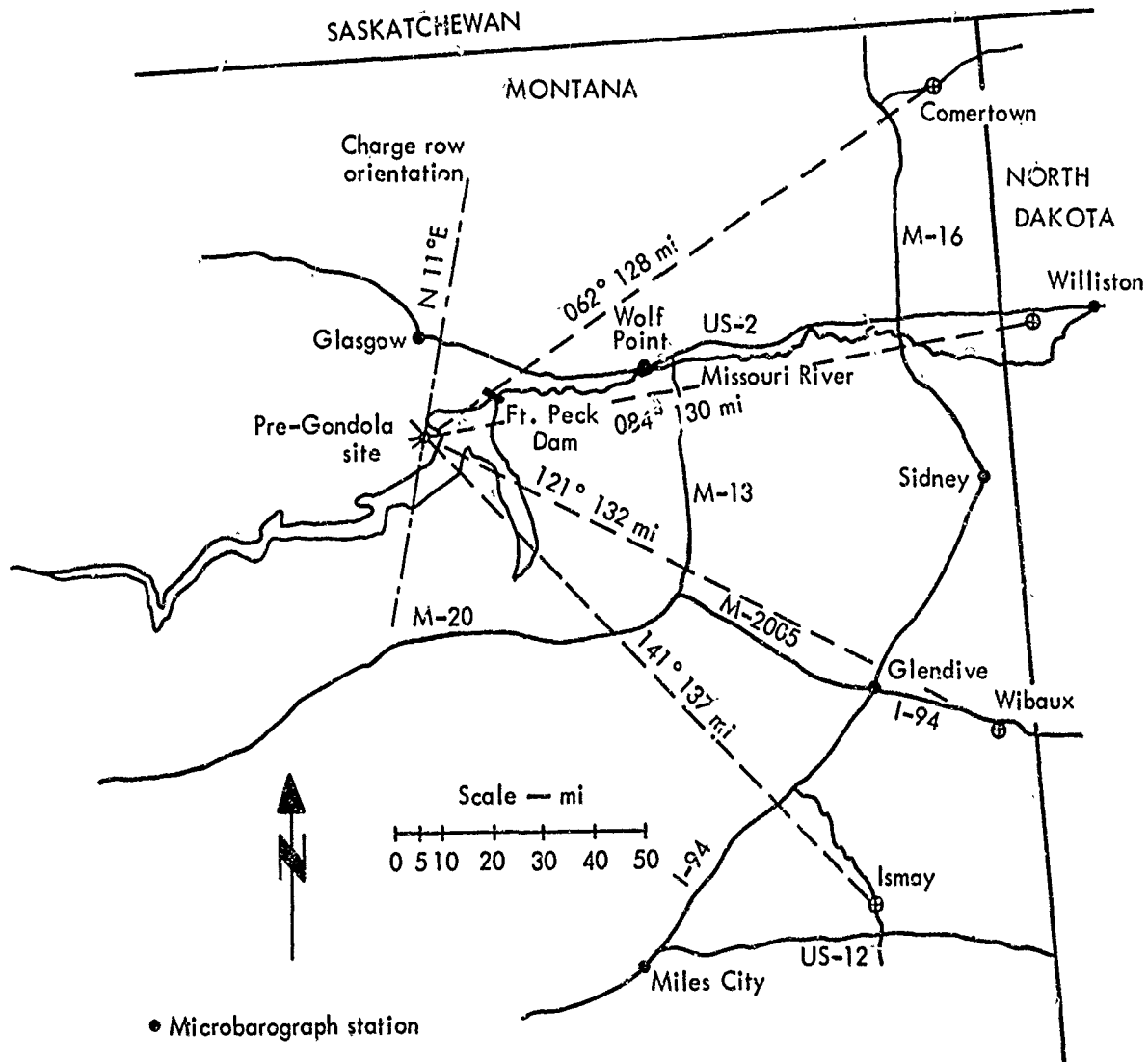| Station | Shot-to-station | | Bearing from Pre-Gondola III axis (deg) |
	Bearing (deg)	Distance (mi)	
Comertown, Montana	062	128	052
Williston, North Dakota	084	130	073
Wibaux, Montana	121	132	110
Ismay, Montana	141	137	130

Fig. 1. Pre-Gondola site and microbarograph locations.

were not surveyed for this project, because map measurements were considered accurate enough for purposes of blast propagation interpretation.

The microbarographs were the same equipment units which have been used on many other explosives tests.[8] A ring of snowfence was placed around each sensor to reduce ambient wind noise. A 3-m radius fence appears to cut wind noise amplitudes by a factor of at least 5 or 6, without significantly affecting the coherent blast-wave signal.[9]

To establish what atmospheric propagation conditions existed at test event time and what airblast amplitudes would be scaled for other known source strengths under these conditions, three calibration shots were fired. These were detonated in an area about 1 mi north from Pre-Gondola III, Phase II, at H-2 min, H+3 min, and H+5 min. Each calibration shot was 2500 lb of Composition-B explosive, placed on a 15-ft high wood-frame platform. This height-of-burst has been used for calibration shots in recent years to give enhanced and repeatable airblast strength.

When 2500 lb of Composition-B HE is detonated 15 ft above ground, height-of-burst effects give an airblast equivalent (or apparent) yield, W_a, of 2.52 tons of HE in a free-air burst, or 5.04×10^{-3} kt of nuclear (NE) free-air burst.[10]

The peak-to-peak recorded pressure amplitude, p_k^* (in millibars), at a measuring station for hemispherical blast wave expansion in a homogeneous, calm atmosphere, with no refraction and extending beyond the distance range of hydrodynamic calculations in IBM Problem M,[11] is given by:

$$p_k^* = 962\ W_a^{0.4}\ R^{-1.2}$$

where

R = range in thousands of feet

W_a = apparent yield in kilotons

For the calibration detonations, then,

$$p_k^* = 115.9\ R^{-1.2}. \tag{1}$$

In this equation, incident amplitude, p_k, has been doubled by ground reflection to give recorded amplitude, p_k^*.

Standard propagation amplitudes are shown in Table 2, both for sea level standard ambient pressure and (as scaled) for ambient pressure at microbarograph elevation.[12,13]

Actual recorded amplitudes from these calibration shots reflect an atmospheric refractive convergence or divergence of energy, known as the focus factor. A focus factor is obtained from each wave recording by dividing recorded amplitude by the standard propagation amplitude. Standard propagation amplitudes are shown in Table 2. The focus factor is assumed to be independent of yield and a function of atmospheric conditions only. Thus for some other yield, such as a cratering test event, a new standard amplitude may be scaled and multiplied by this focus factor to give an amplitude expected for the test yield, free-air burst, at the same time and place as the calibration shot. This expected amplitude, divided by the actual recorded underground event amplitude, gives the muffling factor or attenuation applied by that underground environment. The inverse is known as the transmission factor.

Based on Nevada Test Site (NTS) experience,[7] propagations downwind with ozonosphere ducting show an average focus factor of about 1.0. Thus average amplitudes about equal standard amplitudes.

-3-

Table 2. Standard propagation amplitudes for calibration shots (2500 lb of Composition-B, 15-ft height-of-burst).

Station	Range (10^3 kt)	Altitude (ft) MSL	Standard atmosphere pressure (mbar)	Sea level p_k^* (μbar)	Altitude p_k^* (μbar)	Expected range (μbar)
Comertown	676	2300	932	46.6	44.7	20-100
Williston	686	2325	931	45.8	43.9	20-98
Wibaux	697	2770	918	44.9	42.6	18-95
Ismay	723	2440	927	43.0	41.1	18-92

There is, however, an expected log-normal scatter factor or geometric standard deviation, σ_G = 2.2, where standard deviation, $\sigma = \ln \sigma_G = \pm 1.246$.[14] Typical transmission factors, from previous HE cratering tests, may range from approximately 0.05 to 0.30.

The Environmental Science Services Administration (ESSA)* support detachment from the Las Vegas Research Station made a shot-time rawinsonde balloon ascension to measure temperatures and winds to about 90,000-ft MSL altitudes.[15] A shot-time sounding of upper-air wind and temperature conditions, by rawinsonde, allows an acoustic ray-path calculation which gives another estimate of the atmospheric focus factor.[16] This calculated value is compared to calibration shot recordings to evaluate predictive capabilities.[17] It also aids in identifying and interpreting recorded signals, and in establishing the existence of signals which are near the amplitude of ambient noise.

Results

All operations critical to microbarograph measurements were successful. The Pre-Gondola III Phase II event was fired on schedule, as were all three HE calibration shots. ESSA successfully launched a shot-time rawinsonde balloon for upper air data. All four microbarograph stations were operating satisfactorily, in low wind noise backgrounds, and recorded signals from all four detonations.

Microbarograph records were read, and amplitudes and descriptions of the various signals are listed in Table 3. Maximum amplitude signals for each station and shot were selected and averaged to give a mean focus factor of only 0.73. This weak propagation may be typical of the early winter circulation in the high stratosphere and would be expected to increase as winter sets in. Amplitudes of ozonosphere signals are plotted in Fig. 2, and compared with the standard propagation curve. These data show large scatter which is typical for these measurements.

---

*Now designated NOAA for National Oceanographic and Atmospheric Administration.

Table 3. Summary of microbarograph recordings.

Station	Signal[a]	Atmospheric duct[b]	Average travel speed (ft/sec)	Peak-to-peak amplitude (μbar)				Atmospheric focus factor		
				Cal-1	PG-III	Cal-2	Cal-3	Cal-1	Cal-2	Cal-3
Comertown	a	T	1109	12.9	12.3	6.3	6.5	0.289	0.141	0.145
	b	Z	942	9.3	32.9	41.0	16.9	0.208	0.917	0.378
Williston	a	T	1120	12.2	19.0	14.0	15.8	0.278	0.312	0.360
	b	Z	965	22.5	25.9	11.3	8.9	0.513	0.257	0.203
	c	Z	963	18.2	20.9	31.8	34.9	0.415	0.724	0.795
	d	Z	958	27.8	53.7	54.0	51.5	0.633	1.251	1.173
Wibaux	a	Z	996	14.8	86.9	28.6	24.4	0.347	0.671	0.573
Ismay	a	Z	997	20.8	82.2	26.5	24.9	0.506	0.645	0.606
	b	Z	993	27.3	34.7	35.1	31.0	0.664	0.854	0.754
	c	Z	989	21.8	21.6	44.1	27.9	0.530	0.073	0.579

[a] The letters a, b, c, d indicate successive arrivals of wave packets which have travelled to different altitudes at differing average speeds.

[b] T - troposphere; Z - ozonosphere.

Amplitude variability for calibration shots was analyzed statistically, and lognormal or geometric standard deviations are plotted in Fig. 3. Observed variability does not increase monotonically with time interval between shots as might be expected for a weather-dependent variable; i.e., bigger changes would be expected over longer time intervals. This is not significant, however, in comparison with the average geometric standard deviation or scatter factor of 1.78. This average is somewhat larger than has been found for similar experiments at NTS.

Pre-Gondola III, Phase II was heard by people in Glasgow, about 10 mi north of the test site. In Fort Peck, 6 mi east, the blast rattled windows but no damage was reported. None of the summer homes along the lake (at about 3 to 4 mi) suffered window breakage. Workmen building some new cabins confirmed a loud "thump" (but smaller than some sonic booms they had experienced) and reported that they heard no glass breaking. It appeared that no serious and unexpected atmospheric ducting had occurred, although there were westerly winds and slight ducting in the atmospheric boundary layer.

Excerpts from the ESSA weather summary[15] are shown in Table 4, which gives temperatures and winds at selected altitudes for sound ray calculations. There was a weak temperature inversion extending to a height of about 1000 ft above ground, and WNW winds became light northerly above it. Further aloft, winds shifted gradually with height and increased to a jetstream maximum of 80 kts from the southwest at 35,000 ft MSL. Above the tropopause, at about 50,000 ft MSL, winds dropped to light and variable. There is no rocket sounding station in this vicinity to give upper stratosphere circulation, as is possible with Tonopah Test Range soundings for NTS events.

Sound velocity (sound speed* plus the directed wind component) vs altitude is shown in Fig. 4 for bearings toward the four microbarographs. The only calculated ducting was in the boundary layer,

_____
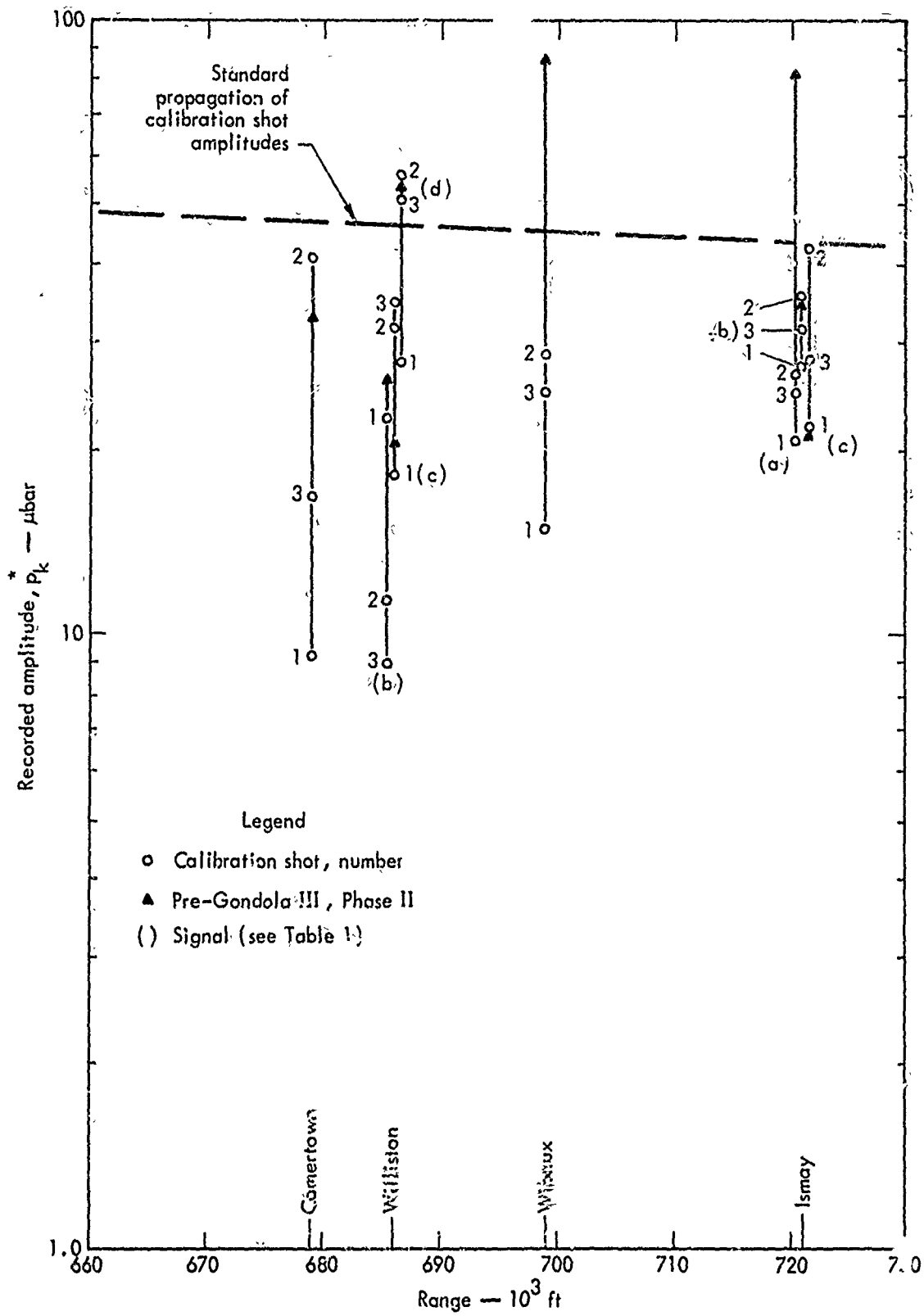*Sound speed is determined by atmospheric temperature.
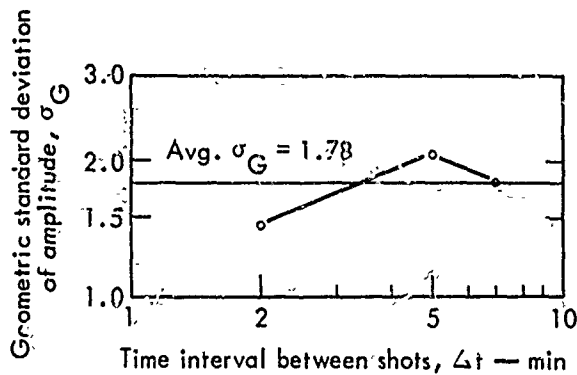
Fig. 2. Ozonosphere signal amplitudes.

Fig. 3. Variability of calibration shot amplitudes.

Table 4. Pre-Gondola III Phase II rawinsonde data.[15]

Altitude (ft) MSL	Temperature (°C)	Wind (deg/knots)
2,349[a]	15.8	300/9
2,930	13.9	300/11
3,250	15.7	310/11
5,000	13.8	360/3
6,000	12.5	340/5
7,000	9.5	290/10
10,000	3.2	260/15
12,000	-1.8	270/18
15,000	-9.6	230/17
20,000	-16.3	230/37
25,000	-27.5	220/50
30,000	-39.5	220/61
35,000	-49.5	220/80
45,000	-54.6	200/63
50,000	-59.3	210/40
60,000	-53.0	240/2
70,000	-52.2	240/2
80,000	-48.2	010/8
90,000	-44.2	020/11

[a]Surface burst height.

below 1000 ft, toward 084-, 121-, and 141-deg bearings. No ducting was shown for the 062-deg bearing. Details of this low-level structure are reproduced in larger scale in Fig. 5, but using as hor-

izontal coordinate the sound velocity differences compared to ground level values. This figure better illustrates the velocity increases necessary to give sound ducting at various altitudes; i.e., $(V_z - V_0) > 0$. Also, propagations in this boundary layer should travel around 1130 ft/sec. This calculation does not explain troposphere signals recorded at Comertown and Williston that traveled at 1109 and 1120 ft/sec, respectively.

It appears that an effective ducting wind probably occurred near 20,000 ft MSL. There could have been a gust leading to a sound velocity greater than V_0 in some localized strata not detected by the rawinsonde balloon. Since troposphere waves were not detected by southeast stations toward which boundary layer ducting was stronger and since they were nearly crosswind to the jet stream, this explanation seems reasonable.

Ozonosphere waves, indicated in Table 3, are not confused with tropospheric propagations because they arrive so much later. Group velocities, defined simply as range divided by arrival time, are plotted vs range in Fig. 6. From inspection of Fig. 4 it is clear that these late arrivals must have traveled a considerable distance in the cold tropopause region and taken a much longer path to the microbarographs. The pattern of arrivals in Fig. 6 is quite typical of experience at NTS, because group velocity is larger at more distant stations. Paths to closer stations reach about the same peak altitude but bend back to the ground at shorter range. Thus they have greater curvature so that horizontal propagation velocity components average smaller than they do for greater ranges.
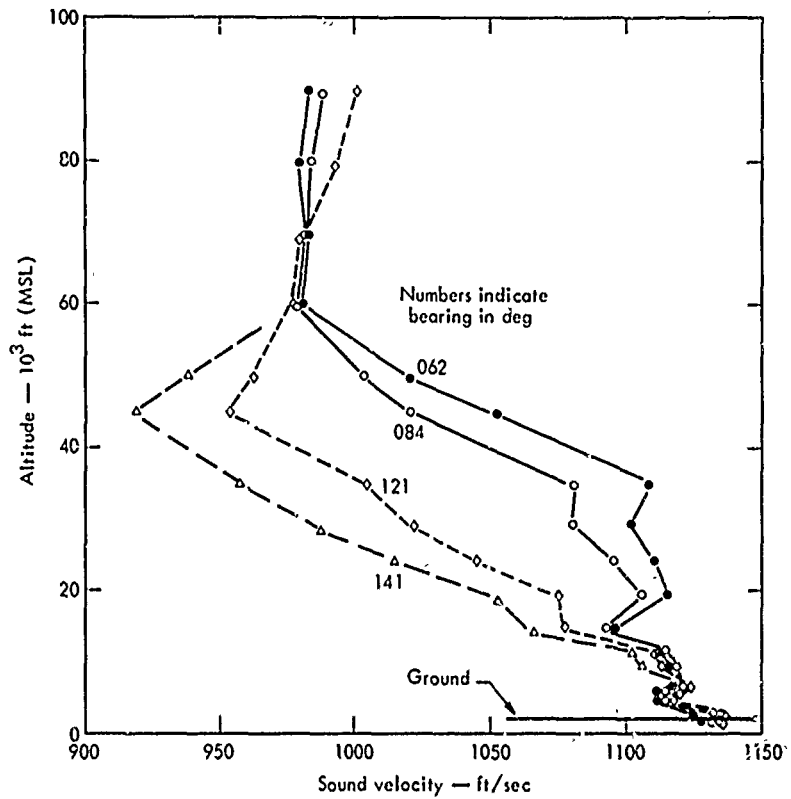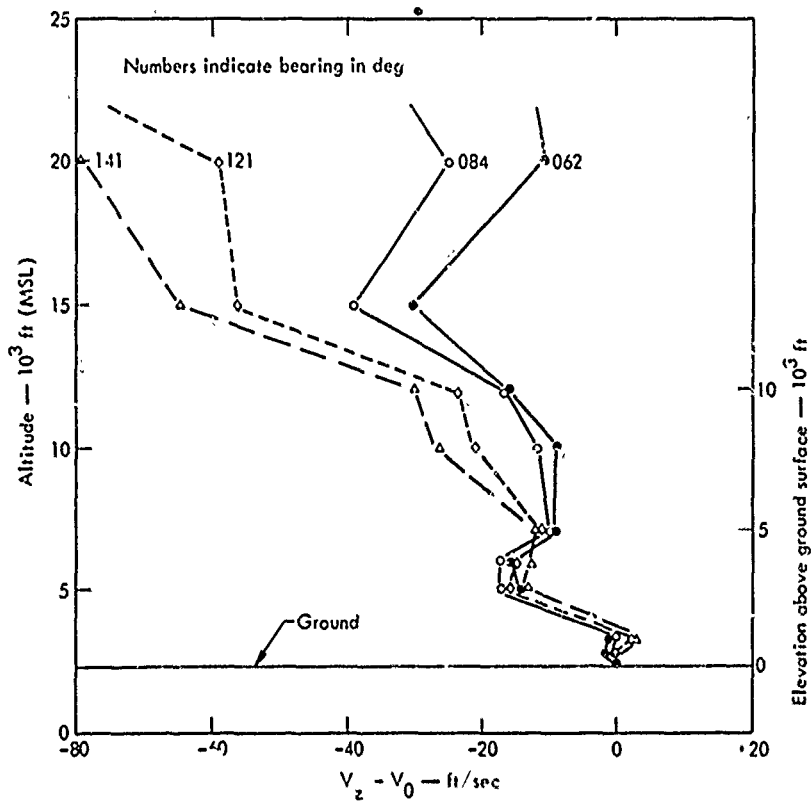
-7-

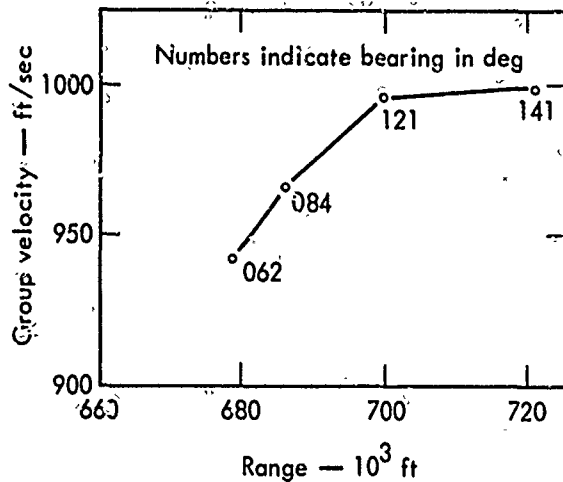Fig. 4. Sound velocity vs altitude.

Fig. 5. Ducting velocity vs altitude.

Fig. 6. Wave arrival velocity vs range.

Transmissivity and Row-Charge Effects

Transmissivity or transmission factor, T, for underground explosions is a function of burst medium and scaled depth of burst and is defined[2] as the ratio of observed airblast amplitude to that expected at the same distance from the same yield burst in free air with the same atmospheric conditions. For underground bursts, Eq. (1) becomes

$$p_k^* = 962 \, W^{0.4} \, R^{-1.2} \, T, \qquad (2)$$

for bursts in a homogeneous calm atmosphere. This is multiplied by the atmospheric focus factor, F, for bursts in a real atmosphere, so that

$$p_k^* = 962 \, W^{0.4} \, R^{-1.2} \, TF. \qquad (3)$$

Row charges emit enhanced airblasts which have been empirically determined to depend on a power of the number of charges in the row, "n," and the yield of a single charge in the row, W_i, as

$$p_k^* = 962 \, n^{\alpha} \, W_i^{0.4} \, R^{-1.2} \, TF. \qquad (4)$$

If acoustic amplitude addition were effective, $\alpha = 1$, while if yield addition were assumed for a source, $\alpha = 0.4$. Experi-

ments have shown that a compromise occurs, that $\alpha \approx 0.7$ in directions perpendicular to the row,[6] but there is still considerable uncertainty regarding this exponent. Also, off row ends, it appears that $\alpha \approx 0.25$. The form of this exponent change with bearing is not obvious but some trigonometric form may be assumed.

Thus, by comparing recorded waves from airburst calibration shots of yield $W_a(Cal)$ with cratering explosives of single charge yield $W_i(Cr)$, fired close in space, $R(Cal) \approx R(Cr)$, and in time, $F(Cal) \approx F(Cr)$, transmissivity and row charge effects are related by:

$$T = \frac{p_k^*(Cr)}{n^{\alpha} p_k^*(Cal)} \left[\frac{W_a(Cal)}{W_i(Cr)} \right]^{0.4}. \qquad (5)$$

Evaluating for Pre-Gondola III, with $W_i(Cr) = 30$ tons NM $\approx$ 33 tons HE, and $W_a(Cal) = 2.52$ tons HE free-air burst, gives:

$$T = \frac{0.357 \, p_k^*(Cr)}{7^{\alpha} p_k^*(Cal)}. \qquad (6)$$

-9-

Table 5. Signal amplitude ratios, normalized for yield.

Station	Signal[a]	Atmospheric duct[b]	$7^\alpha T = 0.357\, p_k^*(Cr)/p_k^*(Cal)$		
			Cal-1	Cal-2	Cal-3
Comertown	a	T	0.341	0.698	0.676
	b	Z	1.264	0.287	0.696
Williston	a	T	0.557	0.485	0.430
	b	Z	0.411	0.819	1.040
	c	Z	0.410	0.235	0.214
	d	Z	0.690	0.350	0.373
Wibaux	a	Z	2.099	1.086	1.273
Ismay	a	Z	1.412	1.109	1.180
	b	Z	0.454	0.353	0.400
	c	Z	0.354	0.175	0.277

[a]The letters a, b, c, d indicate successive arrivals of wave packets which have travelled to different altitudes at differing average speeds.

[b]T - troposphere; Z - ozonosphere.

Pressure ratios, multiplied by 0.357, have been calculated for each recorded wave in Table 5, and plotted vs bearing from the row-charge axis in Fig. 7. A prediction curve is shown based on T = 0.2 from Sedan and $\alpha = 0.475 + 0.225 \cos 2\theta$ (where θ is the bearing angle from the perpendicular), which yields (α, θ) values of (0.25, 90 deg) and (0.7, 0 deg). Also an RMS cosine curve fit was calculated for ozonosphere signals and is shown by a dashed line. Including the troposphere data would little affect this result. Data scatter is so great as to obscure any basis for choice between the two curves. Nor is it possible to separate the variable (θ, T)

from the RMS solution. Expectations are also indicated for a single 33-ton HE burst and for one of 7 × 33 = 231 tons of HE. This latter value is exceeded by about 30% by the data average, but this is not necessarily significant with such large data scatter.

Calculation of log-normal standard errors from these data gives an error factor of $(1.98)^{\pm 1}$ for the RMS curve, $(2.01)^{\pm 1}$ for the preshot prediction curve, and $(2.07)^{\pm 1}$ for the total yield, single source assumption. In consequence, output from Pre-Gondola III was not found to be significantly different from that expected from the pre-existing model for row-charge cratering explosions.
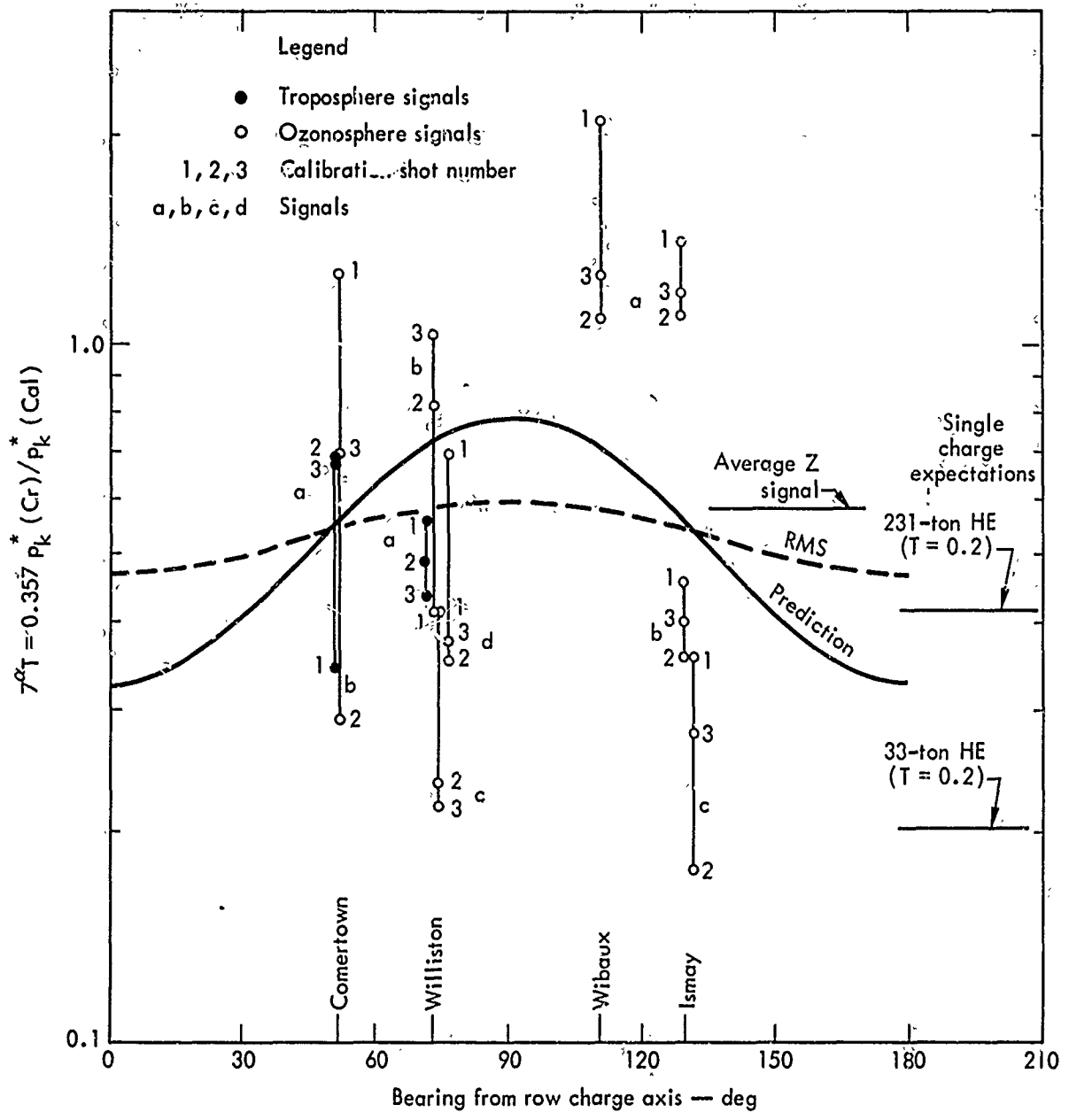
Fig. 7. Normalized amplitude ratios vs bearing angles.

Conclusions

It appears, from these data, that row-charge effects and relations to azimuthal bearing, as determined by close-in measurements and with confidence limited by the typical large data scatter, may be propagating to the great distances of concern to airblast off-site safety. With so much natural, unavoidable scatter in the results, confident extrapolations would require a considerably larger statistical data base.

-11-

References

1. J. E. Lattery, G. C. Steinhardt, B. D. Anderson, J. B. Andrews, B. B. Redpath, J. W. Reed, and R. F. Ballard, Project Pre-Gondola III Phase II Summary Report: Connecting Row-Crater Experiment, U.S. Army Engineer Explosive Excavation Research Office, Livermore, Rept. PNE-1117 (1970).

2. J. W. Reed, Acoustic Wave Effects Project: Airblast Prediction Techniques, Sandia Laboratories, Albuquerque, Interoceanic Canal Studies Report, SC-M-69-332 (1969).

3. J. W. Reed, Multiple Row-Charge Blast-Wave Observations at Long Range, Project Dugout, Sandia Laboratories, Albuquerque, Rept. PNE-607F (1966).

4. L. J. Vortman, Close-in Airblast from the Buggy Event, Sandia Laboratories, Albuquerque, Rept. PNE-320 (1970).

5. L. J. Vortman, Comparison of Air Blast from Two Sizes of Row Charges, Sandia Laboratories, Albuquerque, Rept. SC-RR-66-415 (1966).

6. L. J. Vortman, Airblast and Craters from Rows of Two to Twenty-Five Buried HE Charges, Sandia Laboratories, Albuquerque, Rept. SC-RR-68-655 (1968).

7. J. W. Reed, Climatology of Airblast Propagation from Nevada Test Site Nuclear Airbursts, Sandia Laboratories, Albuquerque, Rept. SC-RR-69-572 (1969).

8. J. A. Maxim, J. W. Reed, and F. Shoemaker, Microbarograph Operations Manual, Sandia Laboratories, Albuquerque, Rept. SC-4942(M)(1964)(OUO).

9. B. A. Bodhaine, Wind Attenuators for Microbarograph Measurements, Sandia Laboratories, Albuquerque, Rept. SC-TM-65-469 (1965).

10. L. J. Vortman and J. D. Shreve, Jr., The Effect of Height of Explosion on Blast Parameters, Sandia Laboratories, Albuquerque, Rept. SC-3858(TR) (1956).

11. C. D. Broyles, IBM Problem M Curves, Sandia Laboratories, Albuquerque, Rept. SCTM 268-56(51) (1956).

12. R. G. Sachs, The Dependence of Blast on Ambient Pressure and Temperature, Ballistic Research Laboratory, Aberdeen Proving Ground, Maryland, Rept. 466 (1944).

13. The Effects of Nuclear Weapons, S. Glasstone, Ed. (U.S. Gov't Printing Office, Washington, D. C., 1962), DOD/AEC, rev. ed.

14. J. Aitchison and J. A. C. Brown, The Log-Normal Distribution (Cambridge University Press, New York, N. Y., 1963).

15. Project Pre-Gondola III Weather Support, ESSA-ARL, Las Vegas, Nevada, February 1969.

16. R. J. Thompson, Computing Sound Rays in the Presence of Wind, Sandia Laboratories, Albuquerque, Rept. SC-RR-67-53 (1967).

17. J. W. Reed and H. W. Church, Sedan Long-Range Blast Propagation, Project Plowshare, Sandia Laboratories, Albuquerque, Final Report PNE-202F (1963).